URTeC: 1922843

Where Did The Proppant Go?

Jonathan P. McKenna* MicroSeismic, Inc.

Introduction

Effective propped fracture half-lengths following a typical hydraulic fracture stimulation of a wellbore can be difficult to quantify. Therefore, different techniques for modeling proppant distributions must be applied to the same dataset for validation purposes and to gain insight into the actual proppant distributions. A proppant-filled fracture model is applied to one well targeting the Evie Member of the Horn River Formation (British Columbia, Canada). Another technique for identifying microseismic signatures associated with the initial slickwater pad and the proppant-laden fluid was applied to the same well to obtain observed proppant distributions. The similarity of the proppant distributions from the two techniques gives validation to each procedure and the results can be used to optimize future completion techniques.

Theory: Fracture Modelling

The seismic moment (M_0), which is defined as $A\mu\delta$ (A is area of the slip plane, μ is shear modulus, and δ is average displacement along the slip plane), is a fundamental equation that relates seismic source parameters to actual measured variables (Kanamori, 1977). McGarr (1976) related total detected seismicity to injected volumes assuming that the change in volume is completely accommodated by the seismic failure using the equation $\sum M_0 = k\mu|\Delta V_i|$ where k is a scaling factor ranging from 0 to 1 which could account for fluid leaking off into the formation. This leakoff volume can be determined from a Diagnostic Fracture Injection Test (DFIT) by $\eta = \frac{V_f}{V_i}$ where η is termed the fluid efficiency, ranging 0-1, where a value of 1 indicates that all of the injected fluid (V_i) is reflected by an identical fracture volume (V_f) and when η is equal to 0, all of the fluid is assumed to leakoff into the formation. Since $V_f = A\Delta u$ (Δu is the opening of the fracture that is empirically related to the length of the fracture using a power law relation (e.g. Vermilye and Scholz, 1995), $V_f = A\Delta u = V_i\eta k$ where k in this case accounts for any undetectable seismic failure. Assuming an aspect ratio (e.g. for an aspect ratio of 0.5, fracture height, h, is 0.5L where L is the length of the fracture) the geometry of each fracture with a hypocenter seismic moment (M_0) can be calculated. Displacement is initially estimated as a function of M_o by assuming a constant stress drop of 3 MPa using data by Bohnhoff et al. (2010).

Next the scaling factor, k, is calculated. This scaling factor is intended to account for any missing seismic population (e.g. tensile fractures that emit rapidly attenuating low frequency signal and microseismic events with signal below the microseismic acquisition geometry and processing methodology detection threshold). The value of k is calculated on a stage by stage basis and choose a calibration stage as the stage with the highest k value (V_f is closest in value to V_i). However, k is chosen for a calibration stage when the microseismicity for that stage is associated with deformation induced from injecting fracture fluid (e.g. rock-stress and fluid-induced fractures). Therefore, stages that contain tectonically-induced fractures (e.g. b-values < 2 (Wessels et al., 2011)) are eliminated. Once the appropriate k-value is chosen, it is multiplied by the initial estimation of displacement using $d_{new}=dk^{4/5}$, refining the value and each variable describing the fracture geometry is recalculated (e.g. McKenna and Toohey (2013). In this way, V_f now equals $V_i\eta$ for the calibration stage and $V_f < V_i\eta$ for all other stages. The value

of scaling up fracture size using *k* is that the *D*-value (which describes the overall shape or dimension of the event cloud (e.g. Hirata et al., 1987)) is preserved as we are using the existing event locations and not adding in new events to account for any missing seismic population. The initial and final displacement estimates are in a range of values that suggest a stress drop of approximately 3-0.1 MPa for a -1 magnitude microseism which seem reasonable according to published data by Bohnhoff et al (2010). After the fracture network is calibrated, the fractures can then be filled with the measured injected proppant volume on a stage-by-stage basis by initially filling fractures nearest the wellbore and systematically filling fractures outward from the wellbore until all deposited proppant volumes have been depleted.

Fracture Modeling Measurements and Results

Direct and indirect measurements were used to calculate the Discrete Fracture Network (DFN) geometry and orientation of the fractures including M_o, μ, η, V_i, δ and the hypocenter focal mechanism (e.g. McKenna and Toohey (2013). Seismic moment and magnitude are measured for each microseismic event and the focal mechanism for each event is used to determine the orientation of each fracture. Well logs are used to calculate μ as a function of depth which is paired to the hypocenter occurring at the respective depth. DFIT tests are interpreted to calculate η for the formations of interest. The actual pumped volumes, V_i, are calculated for each treated stage using the clean total volume plus the proppant volume.

Figure 1 shows the modeled propped and unpropped fractures of the example Evie well and Figure 2 shows a histogram of proppant distribution using the DFN modeling approach with respect to the perpendicular distance from the stage center (black columns). These results can be used to design for future well and stage spacing as well as the optimal depth to land future wells.
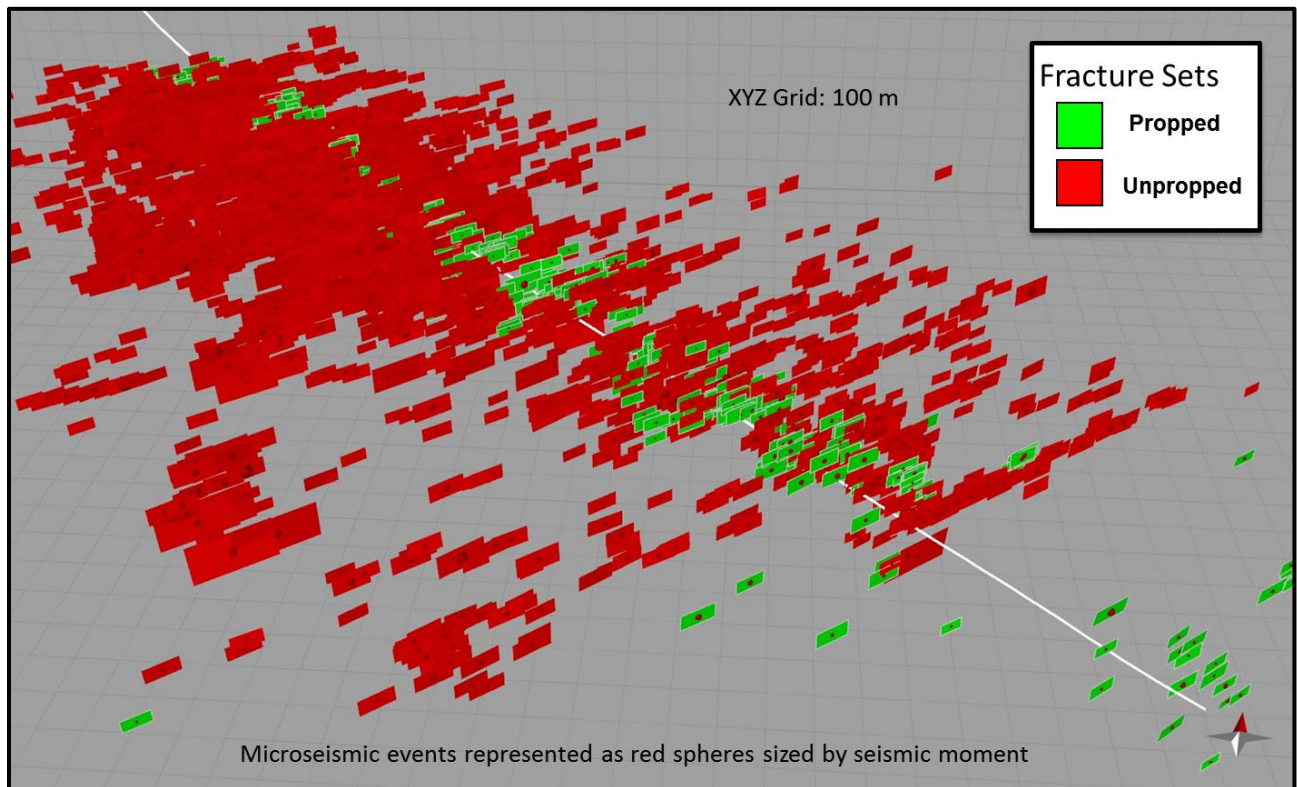
Figure 1: Oblique view of modelled fractures. Fractures are oriented by focal mechanisms and clored green if propped and red if unpropped. Microseismic events are colored red and sized by seismic moment.
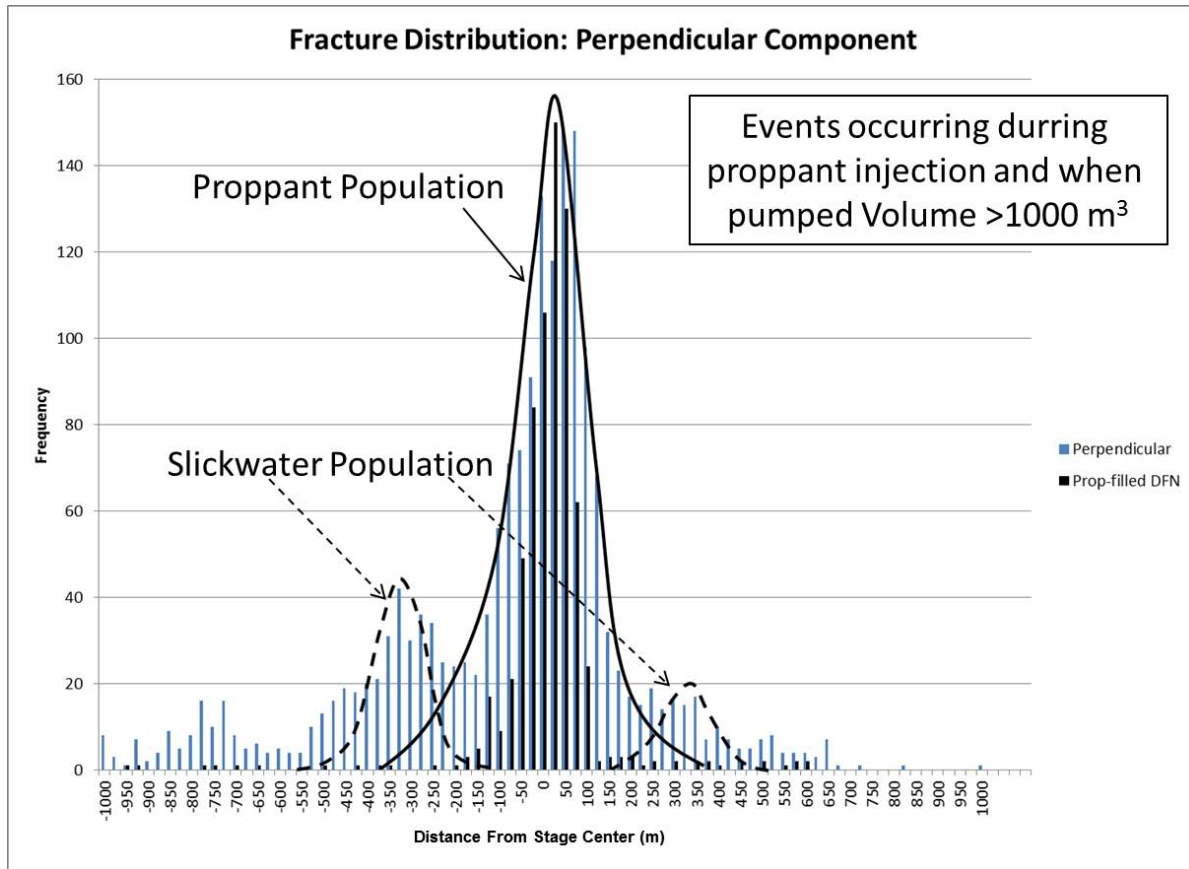
Figure 2: Comparison of proppant population using the perpendicular microseismic location using the treatment design analysis approach where microseismic events are limited to events occurring during proppant injection and when pumped slurry volume is > 1000 m3 (blue histogram) to modeled proppant-filled Discrete Fracture Network (DFN) modeling approach (black histogram). Proppant population can be separated from slickwater population by assuming that two populations exist and are normally distributed.

Treatment Design Analysis (TDA)

The centroid of a microseismic cloud can be mapped as the treatment progresses by plotting the average microseismic location as a function of average slurry volume using a moving window (~20 m^3). By using all microseisms from each stage of the entire well, we can create a graph depicting what a typical stage looks like. Centroid locations can be separated into three main components with respect to the well orientation and stage center: the horizontal perpendicular and parallel components, and the vertical component.

By tracking the microseismic centroid location throughout the treatment, we can identify engineering parameters that influence the location of the microseisms. The focus of this paper is on proppant placement, so we will only consider the influence of proppant concentration on microseismic location. Although proppant injection influences the microseismic location with respect to each of the three main components, its influence is especially apparent in the horizontal perpendicular component and will be the focus for this study. Figure 3 shows that prior to proppant-injection (slurry volume <600 m^3) microseismicity trends outward from the stage center. However, as bottom-hole proppant concentration increases (0-100 kg/m^3), microseismicity is located closer to the wellbore and the trend line is located closer to the wellbore. When proppant concentration is reduced after the first proppant ramp from 100 to 50 kg/m^3, the trend line grows back out further from the wellbore which is most apparent when slurry volume > 1000 m^3. Similarly, as the second proppant ramp increases in concentration, the trend line moves closer to the wellbore. Finally, after the second proppant ramp reaches a peak and is reduced to 60 kg/m^3, the trend line again moves further from the wellbore. This inverse relation between perpendicular growth of microseismicity and proppant concentration demonstrates that the event location is highly influenced

by proppant concentration. In fact, after proppant is injected, the highest clustering of microseismicity occurs near the wellbore (<100 m) and occurs during highest proppant concentration. One explanation for this phenomena is that the initial slickwater pad (slurry volume < 600 m^3) is used to create the initial fracture network causing consistent outward microseismic growth as slurry volume increases. Then, as the proppant-laden slickwater is introduced (slurry volume > 600 m^3), proppant essentially fills the newly created fractures and microseismicity that is located close to the wellbore is possibly due to localized proppant clogging fractures resulting in rerouting of fluid causing near wellbore complexity or resulting in widening of fractures as the denser fluid fills the fractures and increases pumping pressure.
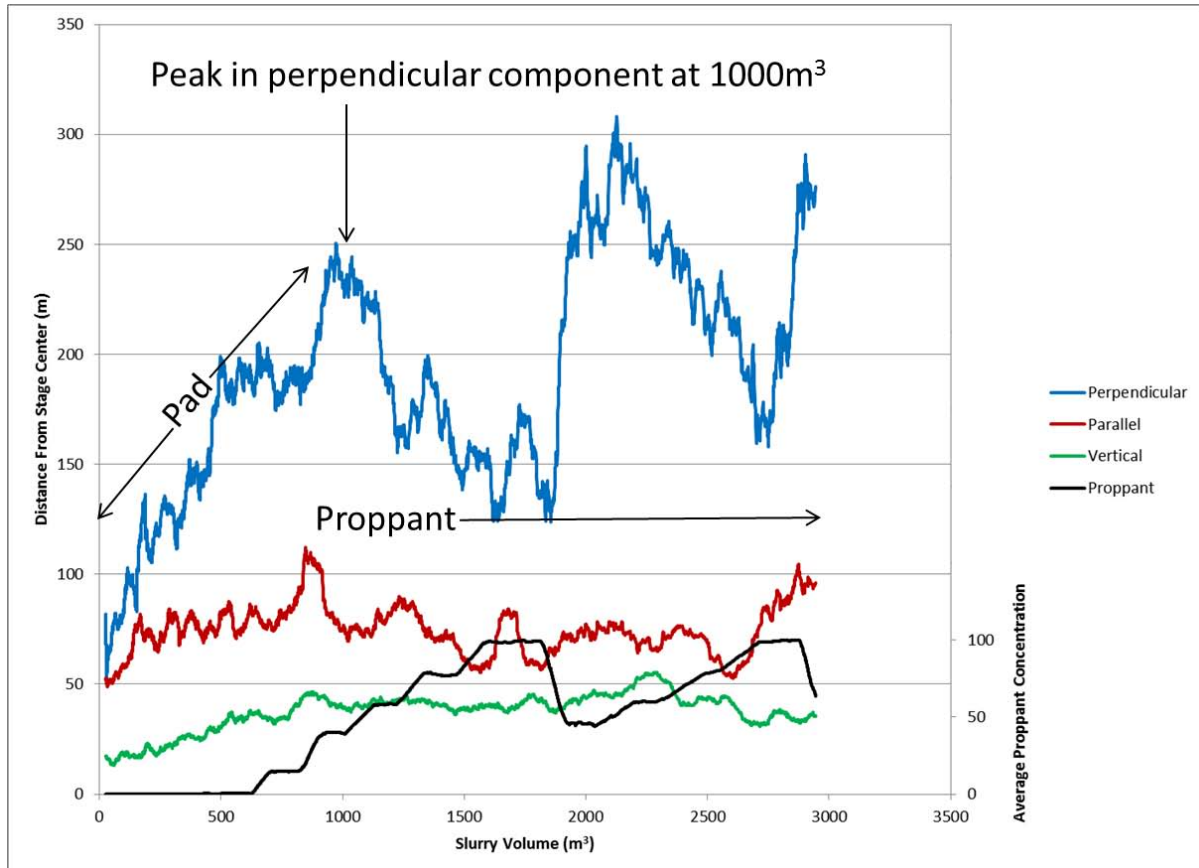
Figure 3: Microseismic growth broken up into perpendicular, parallel, and vertical distances from stage centers (primary y-axis) as a function of pumped volume (x-axis) and proppant concentration (secondary y-axis). Notice that the microseismic location is inversely correlated with proppant concentration indicating that microseismic signature is influenced by proppant injection. During the pad portion of the injection, microseismicity grows outward at a predictable rate from the wellbore reaching a peak in the perpendicular component at ~1000 m^3 and reaches a peak in the parallel and vertical components at ~850 m^3.

Figure 2 shows a histogram of microseismicity in terms of the horizontal perpendicular location with respect to the stage center (blue columns). In an attempt to visualize the microseismicity directly associated with proppant injection, we limit our data to only the events occurring during proppant injection and when slurry volume > 1000 m^3 (after trend line changes slope and begins to grow back toward the wellbore). The histogram shows a main peak close to the center of the stage center and two smaller peaks at approximately +/- 425 m. One hypothesis to explain this distribution is that the slickwater pad that is initially introduced when slurry volume < 600 m^3 propagates outward from the wellbore (Figure 1) and this front continues outward as the proppant is injected and remains out in front of the events due to proppant injection. If we assume that these two populations have a Gaussian distribution, we can roughly sketch out how these two populations are distributed. Interestingly, where the two populations (slickwater and proppant populations) overlap, there are smaller peaks indicating that both

populations are overlapping. Using this technique, we can estimate the distributions of both the slickwater and the proppant populations.

Comparison of Methods

Using Figure 2, the proppant distribution in the perpendicular direction using the proppant-filled DFN model (black histogram) can be compared to the proppant distribution in the perpendicular direction using the treatment design analysis (blue histogram). It is clear that the proppant distributions from both techniques are very similar in shape and distribution and both populations are skewed slightly toward positive values. However, the distribution using the TDA method extends further from the wellbore than the proppant-filled DFN modeling approach. Both techniques yield a median value of 10 m and 88% of the propped fractures using the DFN approach are within 100 m of the wellbore while 72% of the proposed proppant population are within 100 m of the wellbore using the TDA approach. Since both approaches were determined independently, the techniques can be combined to yield a distribution range of how the proppant is distributed.

Discussion

The proppant-filled DFN model accounts for limitations in measureable data and the missing seismic population, and has been verified by similar results from another approach. Improved estimations of δ and η will further improve results. Pressure dependent η can also be incorporated into the methodology since the bottom-hole pressure at the time of microseismic event occurrence can be calculated. Propped fracture distributions using the proppant-filled DFN method described in this paper were compared to propped fracture distributions using the treatment design analysis approach and results were within 18% of one another. This suggests that when these two techniques are combined, the distribution of proppant deposited in a formation following a hydraulic fracture stimulation can be well constrained to yield good estimates.

References

Bohnhoff, M., Dresen, G., Ellsworth, W.L., Ito, H., 2010. Passive Seismic Monitoring of Natural and

Induced Earthquakes: Case Studies, Future Directions ans Socio-Economic Relevance. In: S.

Cloetingh, J. Negendank (eds.), New Frontiers in Integrated Solid Earth Sciences, International

Year of Planet Earth, DOI 10.1007/978-90-481-2737-5_7, Springer.

Hirata, T., Satoh, T and Ito, K., 1987, Fractal structure of spatial distribution of microfracturing in

rock: Geophys. J.R. astr. Soc., 90, 369-374.

Kanamori, H., 1977, The energy release in great earthquakes. Journal of geophysical research, 82

(20): 2981-2987.

McGarr, A., 1976. Seismic moments and volume changes. Journal of geophysical research, 81 (8): 1487-

1494.

McKenna, J.P. and Toohey, N., 2013. A magnitude-based calibrated discrete fracture network

methodology: First Break, v. 31:95-97.

Vermilye, J.M. & Scholz, C.H., 1995. Relation between vein length and aperture, Journal of Structural

Geology, 17, 3, 423-434

Wessels, S. A., De La Pena, A., Kratz, M., Williams-Stroud, S., and Jbeili, T., 2011. Identifying faults and

fractures in unconventional reservoirs through microseismic monitoring, First break, 29 (7): 99-

104.